

**Testing the IONORT-ISP system: a comparison between synthesized
and measured oblique ionograms**

A. Settimi^{a,*}, M. Pezzopane^a, M. Pietrella^a, C. Bianchi^a, C. Scotto^a, E. Zuccheretti^a,
J. Makris^b

^aIstituto Nazionale di Geofisica e Vulcanologia, Via di Vigna Murata 605, 00143, Rome,
Italy

^bTechnological Educational Institute of Crete, P.O. Box 1939 Chania, Crete, Greece

Correspondence to: A. Settimi (alessandro.settimi@ingv.it)

This article has been accepted for publication and undergone full peer review but has not been through the copyediting, typesetting, pagination and proofreading process, which may lead to differences between this version and the Version of Record. Please cite this article as doi: 10.1002/rds.20018

Abstract

The three-dimensional (3-D) electron density representation of the ionosphere computed by the assimilative IRI-SIRMUP-P (ISP) model was tested using IONORT (IONOspheric Ray-Tracing), a software application for calculating a 3-D ray-tracing for high frequency (HF) waves in the ionospheric medium. A radio link was established between Rome (41.8°N, 12.5°E) in Italy, and Chania (35.7°N, 24.0°E) in Greece, within the ISP validity area, and for which oblique soundings are conducted. The ionospheric reference stations, from which the autoscaled f_oF2 and $M(3000)F2$ data and real-time vertical electron density profiles were assimilated by the ISP model, were Rome (41.8°N, 12.5°E) and Gibilmanna (37.9°N, 14.0°E) in Italy, and Athens (38.0°N, 23.5°E) in Greece. IONORT was used, in conjunction with the ISP and the International Reference Ionosphere (IRI) 3-D electron density grids, to synthesize oblique ionograms. The comparison between synthesized and measured oblique ionograms, both in terms of the ionogram shape and the maximum usable frequency characterizing the radio path, demonstrates both that the ISP model can more accurately represent real conditions in the ionosphere than the IRI, and that the ray-tracing results computed by IONORT are reasonably reliable.

Keywords: Electron Density; Ray-Tracing; Oblique Ionogram; IRI; Assimilative Modelling

1. Introduction

Comprehensive, global and regional, features of the Earth's ionosphere are required to ensure the effective planning, operation, and management of numerous radio frequency

systems. As a result, several groups worldwide are actively involved in developing three-dimensional (3-D) models of ionospheric electron density, which after assimilating measured data calculate an updated 3-D image of the ionosphere [Angling and Khattatov, 2006; Thompson *et al.*, 2006; Fridman *et al.*, 2006, 2009; Decker and McNamara, 2007; McNamara *et al.*, 2007, 2008, 2010, 2011; Angling and Jackson-Booth, 2011; Shim *et al.*, 2011].

Pezzopane *et al.* [2011] recently presented a 3-D regional mapping of the ionosphere based on a combination of three main elements: 1) autoscaled data from certain ionospheric reference stations, 2) the $foF2$ and $M(3000)F2$ regional grids calculated by the SIRMUP model [Zolesi *et al.*, 2004; Tsagouri *et al.*, 2005], and 3) the International Reference Ionosphere (IRI) model [Bilitza and Reinisch, 2008]. The procedure was named the IRI-SIRMUP-P (ISP) model. The validity area of the ISP model is the central Mediterranean region extending in latitude from 30° to 44° and in longitude from -5° to 40° , with a $1^\circ \times 1^\circ$ degree resolution, which is exactly the validity area of the regional SIRMUP model. In several studies [Pezzopane *et al.*, 2011, 2012], the ISP model was tested for both geomagnetically quiet and disturbed conditions, demonstrating that in particular at the solar terminator, and under disturbed conditions, the electron densities calculated by the ISP model were more representative of the real conditions of the ionosphere than those calculated using only the climatological IRI-URSI model.

Ray-tracing is a technique to determine the travel path of radio waves from a transmitter to a receiver in an anisotropic and inhomogeneous medium other than vacuum [Budden, 1988]. Bennett *et al.* [2004] reviewed a number of applications and techniques for ray-tracing, mostly from a theoretical point of view. In general, ray-tracing can

accurately be performed if the 3-D electron density distribution between the transmitter and the receiver is known [e.g., *Kashcheyev et al.*, 2012]. Usually, climatological ionospheric models, like IRI, are used to represent electron density distribution. However, since actual electron density distribution can differ significantly from the model, the ray-tracing procedure may return incorrect results. With regard to this issue, Huang and Reinisch [2006] described a real-time high frequency (HF) ray-tracing through a tilted ionosphere. Instead of using an ionospheric model like the IRI, they illustrated a more realistic approach by exploiting a collocated digisonde at the direction-finding site measuring the vertical electron density profile and the local ionospheric tilt, providing, in real-time, the inputs for the construction of the 3-D electron density distribution.

This paper discusses the application of IONORT (IONOspheric Ray-Tracing), a software application for calculating a 3-D ray-tracing of HF waves in the ionospheric medium [*Azzarone et al.*, 2012]. The study considered a number of electron density grids computed by the assimilative ISP model (IONORT-ISP system) and the IRI model (IONORT-IRI system) in order to synthesize oblique ionograms.

Of course, the idea of obtaining artificial oblique ionograms is not new. *Kopka and Möller* [1968] examined theoretical oblique ionograms calculated with a ray-tracing program that included the effects of the Earth's magnetic field. Another interesting finding is that provided by *Gething* [1969] who assumed some simplifying hypotheses, so that the ionosphere was supposed to be composed of stratified concentric spheres with equal electron density. This assumption of spherical stratification, which is equivalent to neglecting ionospheric tilts, is also present in more recent works [*Chen et al.*, 1992].

In principle, IONORT uses a method that does not adopt any of these simplifying hypotheses and it is in line with the state of art results obtained by other groups [e.g. Bamford, 2000]. To test the effectiveness of the IONORT-ISP system, a radio link was established between Rome (41.8°N, 12.5°E) in Italy, and Chania (35.7°N, 24.0°E) in Greece, within the ISP validity area, for which oblique soundings are conducted. The transmitting system is based on a VOS-1 chirp ionosonde produced by the Barry Research Corporation, Palo Alto, California, USA [1975] sweeping from 2 to 30 MHz at 100 kHz/s with an average power of less than 10 W. In this kind of ionosonde the transmitted signal is frequency modulated continuous wave (FMCW) with the result of minimum interference with other users and high noise immunity. The transmitting antenna is a delta for decametric wavelength used for vertical soundings, suited for oblique soundings. The receiver is a RCS-5B chirp produced by the Barry Research Corporation [1989]. The receiving antenna is a Vee sloper loaded oriented towards Rome in order to improve the signal to noise ratio as much as possible.

The ionospheric reference stations used as assimilative sites by the ISP model, in terms of the autoscaled $f\circ F2$ and $M(3000)F2$ data, and the real-time vertical electron density profiles, were Rome (41.8°N, 12.5°E) and Gibilmanna (37.9°N, 14.0°E) in Italy, and Athens (38.0°N, 23.5°E) in Greece (Figure 1).

The comparison, between the synthesized ionograms obtained from the IONORT-ISP and IONORT-IRI systems and the measured oblique ionograms, considered both ionogram shape and maximum usable frequency (MUF) characterizing the radio path, and demonstrated that the ISP model better represents the real conditions of the

ionosphere than the climatological IRI model, and that the ray-tracing results computed by IONORT are reasonably reliable.

2. The IONORT-ISP system: a brief description

Initially, the ISP model checks the autoscaling performed at the ionospheric reference stations. The present study makes use of the autoscaling performed by Autoscala [Pezzopane and Scotto, 2005, 2007; Scotto, 2009; Scotto *et al.*, 2012] on the ionograms recorded by the AIS-INGV ionosonde [Zuccheretti *et al.*, 2003] installed at the ionospheric stations of Rome and Gibilmanna, and by the Automatic Real-Time Ionogram Scaler with True Height analysis (ARTIST) system [Reinisch and Huang, 1983; Reinisch *et al.*, 2005; Galkin and Reinisch, 2008] on the ionograms recorded by the digisonde [Reinisch *et al.*, 2009] installed at the ionospheric station of Athens. If no $foF2$ and $M(3000)F2$ autoscaled values are output from any of the stations, a climatological 3-D electron density grid is computed according to the standard IRI-URSI procedure. By contrast, if at least one station has output autoscaled values of $foF2$ and $M(3000)F2$, the effective sunspot number (R_{eff}) [Houminer *et al.*, 1993] is calculated on the basis of these values [Zolesi *et al.*, 2004], and is then used by the Simplified Ionospheric Regional Model (SIRM) [Zolesi *et al.*, 1996] to provide a nowcast of $foF2$ and $M(3000)F2$ on the regional spatial grid of interest.

The $foF2$ and $M(3000)F2$ value grids computed by the SIRMUP procedure are then used as input to the IRI, and a 3-D updated electron density grid is generated. At this point, if at least one ionospheric reference station has a vertical electron density profile associated with the autoscaling of the ionogram trace, an assimilation process of the measured electron density profiles starts, after which a further updated 3-D electron

density grid of values is generated. Equation (1) represents, at a specific height, the assimilation process performed by the ISP procedure [Pezzopane *et al.*, 2011]: the value T of electron density at a generic point $x_i(\lambda_i, \theta_i)$ (with $i=1, \dots, n$, and where λ_i and θ_i are, respectively, the corresponding geographical longitude and latitude) is calculated as follows:

$$T[x_i(\lambda_i, \theta_i)] = \sum_{j=1}^m \left\{ \exp \left(- \frac{(x_i(\lambda_i, \theta_i) - \bar{x}_j(\lambda_j, \theta_j))^2}{2\sigma^2} \right) M[\bar{x}_j(\lambda_j, \theta_j)] + \right. \\ \left. + \left[1 - \exp \left(- \frac{(x_i(\lambda_i, \theta_i) - \bar{x}_j(\lambda_j, \theta_j))^2}{2\sigma^2} \right) \right] I[x_i(\lambda_i, \theta_i)] \right\} ; \quad (1)$$

σ is a parameter of the exponential weight function that can be varied; $I[x_i(\lambda_i, \theta_i)]$ is the value of electron density before assimilating the measured data at the specific height at the generic point $x_i(\lambda_i, \theta_i)$; $M[\bar{x}_j(\lambda_j, \theta_j)]$ (with $j=1^*, \dots, m$, where m represents the number of reference stations, and λ_j and θ_j are, respectively, their corresponding geographical longitude and latitude) is the measured value of the electron density at the specific height at the point $\bar{x}_j(\lambda_j, \theta_j)$ identifying the position of a reference station.

IONORT [Azzarone *et al.*, 2012] is a software application for calculating a 3-D ray-tracing of HF waves in the ionospheric medium, using an integration algorithm derived from the one coded by Jones and Stephenson [1975]. It is based on a system of first order differential equations with Hamiltonian formalism, solved for a geocentric spherical coordinate system and according to the wave vector components, and previously tested using a horizontal homogeneous model [Bianchi *et al.*, 2011]. Figure 2 shows the

graphical user interface (GUI) of IONORT which enables users to modify the input parameters. Users can also change the model representing the ionosphere, with the possibility of considering an analytical standard Chapman modelled ionosphere [Chapman, 1931], or other numerical representations of the ionosphere (see the “Ionospheric Model” frame in Figure 2). As regards the numerical 3-D representation of the ionosphere, the present study considered electron density grids computed both by the IRI and by the ISP models. In this work, IONORT was used, in conjunction with these two different 3-D electron density grids, to synthesize oblique ionograms that were compared with measured oblique ionograms. Figure 3 gives an overall chart of the IONORT-ISP system.

3. The IONORT-ISP system: analysis and discussion

Basically, a ray-tracing algorithm calculates the path of a ray when the transmitter location, the frequency, and the direction of transmission are given, and so it cannot directly calculate the ray paths that arrive at the receiver. The problem is to know, before tracing the ray, in which directions to transmit a ray so that it will arrive at a given receiver. It is possible to specify the initial conditions of a ray, in particular its launch direction, but where it lands is generally not known until after the calculation. To find all the ray paths connecting a transmitter with a receiver requires a very elaborate *homing-in* routine. Nickisch [2008] discussed an extension of Haselgrove’s equations for accurate computation of ray focusing and ray homing, the application of these equations in HF propagation channel modelling, and, finally the geo-location of targets for Over The Horizon (OTH) radars. The same equations can be used to efficiently home a ray to a

desired landing point (incidentally useful for generating synthetic oblique ionograms, or for performing computations on a fixed link).

At present, the IONORT program is not optimized with an automatic homing-in feature. However, IONORT allows users to specify ranges of frequency [F_{START} , F_{END}] (in MHz), elevation [EL_{START} , EL_{END}] and azimuth [AZ_{START} , AZ_{END}] angles of transmission (in degrees), including those rays that are thought to arrive at the receiver. For each sounding frequency, the algorithm goes over a candidate pool of ray elevation and azimuth angles to exit when the ray's landing point is close to the receiver location. To speed up the exhaustive test computations, it is possible to bypass the loop cycle in azimuth angle and use only the azimuth from transmitter to receiver (see Appendix A). During hours of the day in which the ionosphere is characterized by small horizontal gradients, the azimuth angle of transmission can be assumed to be a constant along the great circle path.

Figure 4 shows a comparison between the oblique ionogram recorded over the Rome-Chania radio link on 4 July 2011 at the solar terminator 20:00 UT, and the corresponding ionogram synthesized by the IONORT-ISP system. When generating synthesized ionograms, for the sake of clarity, only the ordinary trace is shown, calculated taking the geomagnetic field into account. Figures 4b,c,d show the ionogram synthesized, without applying the loop cycle in azimuth angle, for different settings of the elevation angle step and of the receiver range accuracy (see Appendix A). With reference to Figures 4b,c,d, the azimuth angle in the Rome-Chania radio link is fixed at 2.1 radians (121.6°) value. Some growing monotonic trends are highlighted by green circles in Figure 4b. Each monotonic trend corresponds to a single elevation while the frequency loop cycle is running. The ordinary ray, apart from its tip, is practically composed of five trends, from

left to right, corresponding to the elevations of 20° , 21° , 22° , 23° , and 24° , respectively; the frequency bands characterizing the five trends are respectively: [4.5-5.1] MHz, [6.3-7.0] MHz, [8.3-9.4] MHz, [9.6-12.0] MHz, and [11.8-13.2] MHz. Moreover, the synthesized ionogram trace is not continuous and till 8.0 MHz presents some gaps. These apparent defects must be attributed to the low resolution (the elevation angle step is set to 1.0°) of the elevation angle loop. In fact, Figure 4c shows that increasing this resolution (the elevation angle step is now set to 0.2°) causes these fictitious trends to disappear, even though overlapping trace segments due to multiple solutions of the ray-tracing are clearly visible. Figure 4d shows that this numerical effect is removed by just increasing the receiver range accuracy (from 1.0% to 0.1%). However, as in Figure 4b, the trace presents again some frequency gaps.

These apparent defects might be attributed to the above observations, namely that the IONORT program is not optimized with an automatic *homing-in* feature, but runs an iterative procedure in frequency and elevation angle that can only produce a discontinuous piecewise trace of the ionogram. If IONORT were optimized with a homing-in feature, then a suitable adaptive procedure would return the ionogram trace as a continuous line.

At the solar terminator, when the ionosphere is characterized by large horizontal gradients, the azimuth angle of transmission has to be varied since the HF ray lies on a geometrical plane that changes its azimuth angle. In others words, if the HF ray at the initial instant of launch lies along the great circle path then at the end the ray is displaced from it. Conversely, it could happen that at the end the HF ray lies on the great circle path although the ray did not lie on it at the instant of launch. These arguments

explain why in Figure 4d, when the azimuth angle of transmission is fixed, then some frequency gaps appear in the ionogram trace. To fill most of those gaps (see Figure 4e), it is sufficient to iterate a nested loop cycle with azimuth angles from 121° to 122° of step 0.2° . Hence, although IONORT is not optimized with a homing-in feature, even one azimuth cycle may produce an ionogram as an almost continuous line.

4. Results and Discussion

Validation results of the proposed IONORT-ISP system will be shown in this section, comparing the synthesized oblique ionograms produced by the system with the oblique ionograms measured along the Rome-Chania radio link, which lies within the ISP validity area, and for which oblique soundings are conducted using a chirp sounding technique. Figure 1 showed the ionospheric reference stations from which autoscaled f_oF2 and $M(3000)F2$ values, and real-time vertical electron density profiles are assimilated by the ISP model. These are Rome, Gibilmanna, and Athens, and so the index m of Eq. (1) is equal to 3^* . Moreover, the ISP electron density grids were calculated by setting $\sigma=3.0$, where this choice of σ follows the preliminary testing phase of the model developed by *Pezzopane et al.* [2011]. For further comparison, synthesized oblique ionograms obtained by applying IONORT to IRI electron density grids are also depicted.

In order to perform this study on synthesized oblique ionograms, a dataset of 33 oblique ionograms recorded over the Rome-Chania radio link in June, July and October 2011 in the daytime, in the nighttime, at sunrise, at sunset, for quiet and moderate geomagnetic activity, was considered. The requirements of the ionograms forming this dataset had to be: a) clarity of the trace, which is essential in order to perform a trace shape comparison

between measured and synthesized ionograms. With regard to this issue, it is worth noting that often the Rome-Chania radio link gives recorded traces that, in addition to not being tagged for polarization, are either noisy or characterized by interference phenomena preventing the user from accurately validating the MUF; b) most of the ionograms had to be recorded at specific times for which both the autoscaling of Athens, and at least one between the autoscaling of Rome and Gibilmanna, were available and essentially correct. These “boundary conditions” strongly decreased the number of measured oblique ionograms forming the test dataset. The requirement b) is necessary to guarantee that the assimilation process was properly performed with data coming from at least two ionospheric stations located close to the two extremities of the radio path. In Section 5 we will see that the assimilation of data coming from only one station, hence from only one extremity of the radio path, can cause a significant overestimation/underestimation of the real MUF.

Figures 5a and 6a show four examples from the dataset considered, differing both in terms of trace shape and the MUF characterizing the radio path. Figures 5b,c and 6b,c show the IONORT-IRI and IONORT-ISP synthesized oblique ionograms, respectively. It is worth noting that, for these examples, even though the ionosphere is not characterized by large horizontal gradients, the loop cycle in azimuth angle was applied. Moreover, as in Figure 4e, the elevation angle step was set to 0.2° and the RX range accuracy was set to 0.1%, and the corresponding synthesized oblique ionograms do not present any discontinuous piecewise trace and/or significant frequency gaps.

Table 1 shows for all the ionograms of the test dataset the measured MUF, the MUF calculated both by the IONORT-IRI and by the IONORT-ISP systems, and their

corresponding differences with the measured one. For each case, the lowest difference, between the modelled (IONORT-IRI or IONORT-ISP) and the measured MUF values, is highlighted in green.

The results of the comparison are also presented in form of a histogram in Figure 7 in terms of the differences [IRI MUF - measured MUF], and [ISP MUF - measured MUF], where IRI MUF and ISP MUF are the MUF values obtained from the IONORT-ISP and IONORT-IRI synthesized oblique ionograms, respectively.

5. Conclusions and future developments

Figures 5 and 6 show that the oblique ionograms synthesized by the IONORT-ISP system are generally better than the oblique ionograms synthesized by the IONORT-IRI system in terms of both the calculated MUF and the trace shape of ionogram. As expected, this means on one hand that the representation of the ionosphere produced by the ISP model is more realistic than the climatological representation produced by the IRI model, and on the other hand that the ray-tracing results performed by the IONORT algorithm are fairly reliable.

The shape of the IONORT-ISP synthesized ionograms, compared to the measured oblique ionograms, is slightly squashed but in general relatively good. In this respect, it is worth noting three interesting features. Firstly, for low frequencies the trace of the observed ionograms is often absent, while by contrast, the trace of the synthesized ionograms is present. This is mostly due to the fact that the synthesized ionograms were computed without taking into account a collision frequency model, along with other radio

electric parameters required to establish the link, hence without considering the absorption affecting low frequencies. To address this issue, the inclusion of a collision frequency model, as well as the development of a procedure able to take into account the presence of horizontal gradients, is planned as a future improvement of the system. It is also worth pointing out that the low frequency parts of an oblique path could be missing also because the antennas do not favour low elevation angles. Secondly, the synthesized ionograms never show additional higher traces due to multiple hop paths, since only one-hop propagation modes were considered. Thirdly, as expected, the synthesized ionograms never show E sporadic layers often visible in the measured oblique ionograms (see Figure 5a).

Table 1 and Figure 7 again confirm that the IONORT-ISP system is more accurate than the IONORT-IRI system in terms of the calculated MUF. However, focusing our attention on Table 1, we see that, for the last two cases forming the test dataset, the MUF values are strongly overestimated by the IONORT-ISP system. This is probably due to the fact that the corresponding ionograms were recorded at the solar terminator, respectively on 9 October 2011 at 5:00 UT and 6:30 UT, hence under very variable ionospheric conditions; but in particular also because data from Rome and Gibilmanna were unavailable and the only reference ionospheric station contributing to the ISP grids was Athens. This overestimation of MUF values provided by the IONORT-ISP system could probably be smoothed out by including additional ionospheric reference stations in the region of interest, especially located around the midpoint of the path considered. Obviously, in order to confirm this and further test the behaviour of the IONORT-ISP

system, more oblique sounding measurements need to be conducted. This could be the subject of a future study.

In summary, the results presented in this paper suggest that: a) the assimilation by IRI of data measured at multiple ionospheric reference stations is very important to obtain as reliable an image of the ionosphere as possible; b) the combination IONORT-ISP, and more generally IONORT, can be proposed as a valid tool for operational use.

Acknowledgments

The authors are extremely grateful to Dr. Bruno Zolesi and Dr. Lj. R. Cander for the useful simulations made by the SIRMUP model, for the interesting pointers on the literature regarding ionospheric models and ray-tracing, and for the helpful discussions about oblique ionograms.

Appendix A

Figures A1a,b show a flowchart of the IONORT-ISP (or IRI) system, calling an OBLIQUE SOUNDING subroutine that produces “SYNTHETIC IONOGRAM.txt” output. The IONORT program runs on a file, named “GRIDPROFILES.txt”, which is the output of the ISP (or IRI) model, reproducing the 3-D electron density grid over the Mediterranean area on a chosen date (in the format dd/mmm/yyyy). IONORT reads an input file, named “RAY TRACING INPUT.ini”, to initialize the default inputs related to all the computational parameters needed by the ray-tracing algorithm, including the

geographical position of the transmitter (TX), represented in a geocentric spherical coordinate system $(R_{TX}, TH_{TX}, PH_{TX})$ (R_{TX} in km, TH_{TX} and PH_{TX} in radians). The coordinates of the transmitter can be expressed in terms of its height $H_{TX}=R_{TX}-R_T$ (in km) from ground level, where $R_T=6371$ km is the averaged radius of the Earth, and in terms of latitude $LAT_{TX}=(180^\circ/\pi)(\pi/2-TH_{TX})$ and longitude $LON_{TX}=(180^\circ/\pi)PH_{TX}$ angles (in degrees).

The program iteratively calculates a ray path for each nested loop cycle K relative to the frequency F_K , the elevation EL_K , and the azimuth AZ_K angles, specified by a frequency-step $F_K=F_K+F_{STEP}$, elevation-step $EL_K=EL_K+EL_{STEP}$, and azimuth-step $AZ_K=AZ_K+AZ_{STEP}$ procedure, with $K=START, \dots, END$ (see Figure A1a). The computing time footprint of a complete IONORT simulation can be estimated as $\Delta t \cdot N_{TOT}$, if Δt is assumed as the computing time of every loop cycle, where $N_{TOT}=N_F \cdot N_{EL} \cdot N_{AZ}$ is the total number of cycles, with $N_F=1+[(F_{END}-F_{START})/F_{STEP}]$ the number of frequencies, $N_{EL}=1+[(EL_{END}-EL_{START})/EL_{STEP}]$ and $N_{AZ}=1+[(AZ_{END}-AZ_{START})/AZ_{STEP}]$ the number of elevations and azimuths respectively. At the end of each K^{th} nested loop cycle, the OBLIQUE SOUNDING subroutine lists the parameters of ray-tracing output, i.e. the geographical position of the arrival point, still represented in the geocentric spherical coordinate system (R_K, TH_K, PH_K) , and also by the corresponding group delay time T_K (in ms). Moreover, the OBLIQUE SOUNDING subroutine reads an input file, named "RECEIVER.txt", to read the geographical position of the receiver (RX), again represented in the geocentric spherical coordinate system, and the tolerated accuracy of the RX position, defined by the triplet of relative errors $(ERROR_R, ERROR_{TH}, ERROR_{PH})$. These relative errors should not exceed the following reasonable upper

limits: $ERROR_R \leq EIMAX$, $ERROR_TH \leq 0.1\%$, $ERROR_PH \leq 0.1\%$. In fact, $EIMAX$, i.e. the component 42 of vector W represented in the input file “RAY TRACING INPUT.ini” used by IONORT (see Table 1 of *Azzarone et al.* [2012]), is defined as the maximum allowable relative error in any single step length for any of the equations being integrated. To get a very accurate (but expensive) ray trace, it is possible use a small $EIMAX$ (about 10^{-5} or 10^{-6}). For a cheap, approximate ray trace, a large $EIMAX$ (10^{-3} or even 10^{-2}) should be used. For cases in which all the variables being integrated increase monotonically, the total relative error can be guaranteed to be less than $EIMAX$. If $ERROR_TH$ and $ERROR_PH$ are less than 0.1%, then the arrival point is displaced from the receiver by not more than a few kilometers. Finally, the OBLIQUE SOUNDING subroutine compares the geographical positions of the arrival point and the receiver, assessing how close the arrival point is to the receiver. More precisely, OBLIQUE SOUNDING subroutine assumes that the target has been reached, or rather that the arrival point may be approximated with the receiver, when it falls within a circle centered on the receiver, of radius defined by the tolerated accuracies ($ERROR_R$, $ERROR_TH$, $ERROR_PH$) of the RX position. Formally, the subroutine evaluates the following logical condition (see Figure A1b):

$$(ABS((R_K - R_{RX})/R_{RX}) \leq ERROR_R).AND.$$

$$ABS((TH_K - TH_{RX})/TH_{RX}) \leq ERROR_TH).AND.ABS((PH_K - PH_{RX})/PH_{RX}) \leq ERROR_PH.$$

If this expression is false, then it means that the transmitter-receiver radio link has not been established at frequency F_K , elevation EL_K , and azimuth AZ_K . In this case, the

OBLIQUE SOUNDING subroutine returns control to the IONORT system, so the K^{th} loop cycle is concluded while the next cycle starts. By contrast, the transmitter and receiver are radio linked and in this case, OBLIQUE SOUNDING updates the MUF variable ($\text{MUF}=F_k$) which, at the end of whole IONORT simulation, will coincide with the MUF of the radio link. Simultaneously, the subroutine stores in the final output file named “SYNTHETIC IONOGRAM.txt”, the values of frequency F_K and group delay T_K that represent the K^{th} ionogram point $P_K=(F_K, T_K)$ relative to the K^{th} cycle giving rise to a transmitter-receiver radio link (see Figure A1b). At the end of the complete simulation, the final output file will include all the N points, $P_{K1}=(F_{K1}, T_{K1})$, $P_{K2}=(F_{K2}, T_{K2})$, ... , $P_{KN}=(F_{KN}, T_{KN})$, composing the ionogram trace of the radio link. It is worth noting that the nested loop cycle in the azimuth transmission angle is optional. If the loop cycle in azimuth angle is not initiated, then the azimuth between the transmitter and the receiver becomes a fixed constant in the ray-tracing, i.e. $AZ_K=AZ_{\text{START}}=AZ_{\text{END}}$, which can be calculated simply by applying spherical trigonometry:

$$\text{tg}(AZ_{\text{START}})=\sin(TH_{\text{RX}})\sin(TH_{\text{TX}})\sin(PH_{\text{RX}}-PH_{\text{TX}})/[\cos(TH_{\text{RX}})-\cos(TH_{\text{TX}})\cos(\Delta_{\text{TX-RX}})], \quad (\text{A1})$$

where

$$\cos(\Delta_{\text{TX-RX}})=\cos(TH_{\text{RX}})\cos(TH_{\text{TX}})+\sin(TH_{\text{RX}})\sin(TH_{\text{TX}})\cos(PH_{\text{RX}}-PH_{\text{TX}}). \quad (\text{A2})$$

Omitting the azimuth cycle is convenient when possible, as the computing time footprint of the complete IONORT simulation is reduced to $\Delta t \cdot N_F \cdot N_{EL}$, with Δt the computing time for every cycle.

References

Angling, M. J., and B. Khattatov (2006), Comparative study of two assimilative models of the ionosphere, *Radio Sci.*, *41*, RS5S20, doi:10.1029/2005RS003372.

Angling, M. J., and N. K. Jackson-Booth (2011), A short note on the assimilation of collocated and concurrent GPS and ionosonde data into the Electron Density Assimilative Model, *Radio Sci.*, *46*, RS0D13, doi:10.1029/2010RS004566.

Azzarone, A., C. Bianchi, M. Pezzopane, M. Pietrella, C. Scotto, and A. Settimi (2012), IONORT: A Windows software tool to calculate the HF ray tracing in the ionosphere, *Comp. Geosc.*, *42*, 57-63, doi:10.1016/j.cageo.2012.02.008.

Bamford, R. (2000), Oblique soundings - Project Final Report, Radio Communication Research Unit, Rutheford Appleton Laboratory, Chilton, Didcot, UK.

Barry Research Corporation (1975), VOS-1A User Manual. Palo Alto, California, USA.

Barry Research Corporation (1989), RCS-5B Chirpsounder Receiver Operating and Service Manual. Palo Alto, California, USA.

Bennett, J. A., P. L. Dyson, and R. J. Norman (2004), Progress in radio ray tracing in the ionosphere, *Radio Sci. Bull.*, *310*, 81-91.

Bianchi, C., A. Settimi, C. Scotto, A. Azzarone, and A. Lozito (2011), A method to test HF ray tracing algorithm in the ionosphere by means of the virtual time delay, *Adv. Space Res.*, 48, 1600–1605, doi:10.1016/j.asr.2011.07.020.

Bilitza, D., and B. W. Reinisch (2008), International Reference Ionosphere 2007: Improvements and new parameters, *Adv. Space Res.*, 42(4), 599–609, doi:10.1016/j.asr.2007.07.048.

Budden, K. G. (1988), *The Propagation of Radio Wave*. Cambridge University Press, Cambridge, UK, pp. 688.

Chapman, S. (1931), The absorption and dissociative or ionizing effect of monochromatic radiation in an atmosphere on a rotating earth. *Proceedings of the Physical Society of London*, 43(1), 26–45.

Chen J., J. A. Bennett, and P. L. Dyson (1992), Synthesis of oblique ionograms from vertical ionograms using quasi-parabolic segment models of the ionosphere, *J. Atmos. Solar-Terr. Phys.*, 54(3-4), 323–331.

Decker, D. T., and L. F. McNamara (2007), Validation of ionospheric weather predicted by Global Assimilation of Ionospheric measurements (GAIM) models, *Radio Sci.*, 42, RS4017, doi:10.1029/2007RS003632.

Fridman, S. V., L. J. Nickisch, M. Aiello, and M. Hausman (2006), Real-time reconstruction of the three-dimensional ionosphere using data from a network of GPS receivers, *Radio Sci.*, *41*, RS5S12, doi:10.1029/2005RS003341.

Fridman, S. V., L. J. Nickisch, and M. Hausman (2009), Personal-computer-based system for real-time reconstruction of the three-dimensional ionosphere using data from diverse sources, *Radio Sci.*, *44*, RS3008, doi:10.1029/2008RS004040.

Galkin, I. A., and B. W. Reinisch (2008), The new ARTIST 5 for all Digisondes, in Ionosonde Network Advisory Group Bulletin 69, pp. 1–8, IPS Radio and Space Serv., Surry Hills, N. S. W., Australia, Available from <<http://www.ips.gov.au/IPSHosted/INAG/web-69/2008/artist5-inag.pdf>>.

Gething, P. J. D. (1969), The calculation of electron density profiles from oblique ionograms, *J. Atmos. Solar-Terr. Phys.*, *31*(3), 347-354.

Houminer, Z., J. A. Bennett, and P. L. Dyson (1993), Real-time ionospheric model updating, *J. Electr. Electron. Eng., Aust.*, *13*(2), 99–104.

Huang, X., and B. W. Reinisch (2006), Real-time HF ray tracing through a tilted ionosphere, *Radio Sci.*, *41*, RS5S47, doi:10.1029/2005RS003378.

Jones, R. M., and J. J. Stephenson (1975), A versatile three-dimensional ray tracing computer program for radio waves in the ionosphere. OT Report, 75–76, U.S. Department of Commerce, Office of Telecommunication, U.S. Government Printing Office, Washington, USA, 185 pp..

Kashcheyev, A., B. Nava, and S. M. Radicella (2012), Estimation of higher-order ionospheric errors in GNSS positioning using a realistic 3-D electron density model, *Radio Sci.*, 47, RS4008, doi:10.1029/2011RS004976.

Kopka H., and H. G. Möller (1968), MUF Calculations Including the Effect of the Earth's Magnetic Field, *Radio Sci.*, 3, 53-56.

McNamara, L. F., D. T. Decker, J. A. Welsh, and D. G. Cole (2007), Validation of the Utah State University Global Assimilation of Ionospheric Measurements (GAIM) model predictions of the maximum usable frequency for a 3000 km circuit, *Radio Sci.*, 42, RS3015, doi:10.1029/2006RS003589.

McNamara, L. F., C. R. Baker, and D. T. Decker (2008), Accuracy of USU-GAIM specifications of foF2 and M(3000)F2 for a worldwide distribution of ionosonde locations, *Radio Sci.*, 43, RS1011, doi:10.1029/2007RS003754.

McNamara, L. F., J. M. Retterer, C. R. Baker, G. J. Bishop, D. L. Cooke, C. J. Roth, and J. A. Welsh (2010), Longitudinal structure in the CHAMP electron densities and their

implications for global ionospheric modeling, *Radio Sci.*, 45, RS2001, doi:10.1029/2009RS004251.

McNamara, L. F., G. J. Bishop, and J. A. Welsh (2011), Assimilation of ionosonde profiles into a global ionospheric model, *Radio Sci.*, 46, RS2006, doi:10.1029/2010RS004457.

Nickisch, L. J. (2008), Practical Applications of Haselgrove's Equations for HF systems, *Radio Sci. Bulletin*, 325, 36-48.

Pezzopane, M., M. Pietrella, A. Pignatelli, B. Zolesi, and Lj. R. Cander (2012), Testing the three-dimensional IRI-SIRMUP-P mapping of the ionosphere for disturbed periods, *Adv. Space Res.*, doi: 10.1016/j.asr.2012.11.028.

Pezzopane, M., M. Pietrella, A. Pignatelli, B. Zolesi, and L. R. Cander (2011), Assimilation of autoscaled data and regional and local ionospheric models as input sources for real-time 3-D International Reference Ionosphere modeling, *Radio Sci.*, 46, RS5009, doi:10.1029/2011RS004697.

Pezzopane, M., and C. Scotto (2005), The INGV software for the automatic scaling of foF2 and MUF(3000)F2 from ionograms: A performance comparison with ARTIST 4.01 from Rome data, *J. Atmos. Solar-Terr. Phys.*, 67(12), 1063–1073, doi:10.1016/j.jastp.2005.02.022.

Pezzopane, M., and C. Scotto (2007), The automatic scaling of critical frequency foF2 and MUF(3000)F2: A comparison between Autoscala and ARTIST 4.5 on Rome data, *Radio Sci.*, *42*, RS4003, doi:10.1029/2006RS003581.

Reinisch, B. W., and X. Huang (1983), Automatic calculation of electron density profiles from digital ionograms: 3. Processing of bottom side ionograms, *Radio Sci.*, *18*(3), doi:10.1029/RS018i003p00477.

Reinisch, B. W., X. Huang, I. A. Galkin, V. Paznukhov, and A. Kozlov (2005), Recent advances in real-time analysis of ionograms and ionospheric drift measurements with Digisondes, *J. Atmos. Solar-Terr. Phys.*, *67*(12), 1054–1062, doi:10.1016/j.jastp.2005.01.009.

Reinisch, B. W., I. A. Galkin, G. M. Khmyrov, A. V. Kozlov, K. Bibl, I. A. Lisysyan, G. P. Cheney, X. Huang, D. F. Kitrosser, V. V. Paznukhov, Y. Luo, W. Jones, S. Stelmash, R. Hamel, and J. Grochmal (2009), *Radio Sci.*, *44*, RS0A24, doi:10.1029/2008RS004115.

Scotto, C. (2009), Electron density profile calculation technique for Autoscala ionogram analysis, *Adv. Space Res.*, *44*(6), 756–766, doi:10.1016/j.asr.2009.04.037.

Scotto, C., M. Pezzopane, and B. Zolesi (2012), Estimating the vertical electron density profile from an ionogram: On the passage from true to virtual heights via the target function method, *Radio Sci.*, *47*, RS1007, doi:10.1029/2011RS004833.

Shim, J. S. et al. (2011), CEDAR Electrodynamics Thermosphere Ionosphere (ETI) Challenge for systematic assessment of ionosphere/thermosphere models: NmF₂, hmF₂, and vertical drift using ground-based observations, *Space Weather*, 9, S12003, doi:10.1029/2011SW000727.

Thompson, D. C., L. Scherliess, J. J. Sojka, and R. W. Schunk (2006), The Utah State University Gauss-Markov Kalman filter of the ionosphere: The effect of slant TEC and electron density profile data on model fidelity, *J. Atmos. Solar-Terr. Phys.*, 68(9), 947–958, doi:10.1016/j.jastp.2005.10.011.

Tsagouri, I., B. Zolesi, A. Belehaki, and L. R. Cander (2005), Evaluation of the performance of the real-time updated simplified ionospheric regional model for the European area, *J. Atmos. Solar-Terr. Phys.*, 67(12), 1137–1146, doi:10.1016/j.jastp.2005.01.012.

Zolesi, B., L. R. Cander, and G. de Franceschi (1996), On the potential applicability of the simplified ionospheric regional model to different midlatitude areas, *Radio Sci.*, 31(3), 547–552, doi:10.1029/95RS03817.

Zolesi, B., A. Belehaki, I. Tsagouri, and L. R. Cander (2004), Real-time updating of the simplified ionospheric regional model for operational applications, *Radio Sci.*, 39, RS2011, doi:10.1029/2003RS002936.

Zuccheretti, E., G. Tutone, U. Sciacca, C. Bianchi, and B. J. Arokiasamy (2003), The new AIS-INGV digital ionosonde, *Ann. Geophys. Italy*, 46(4), 647–659.

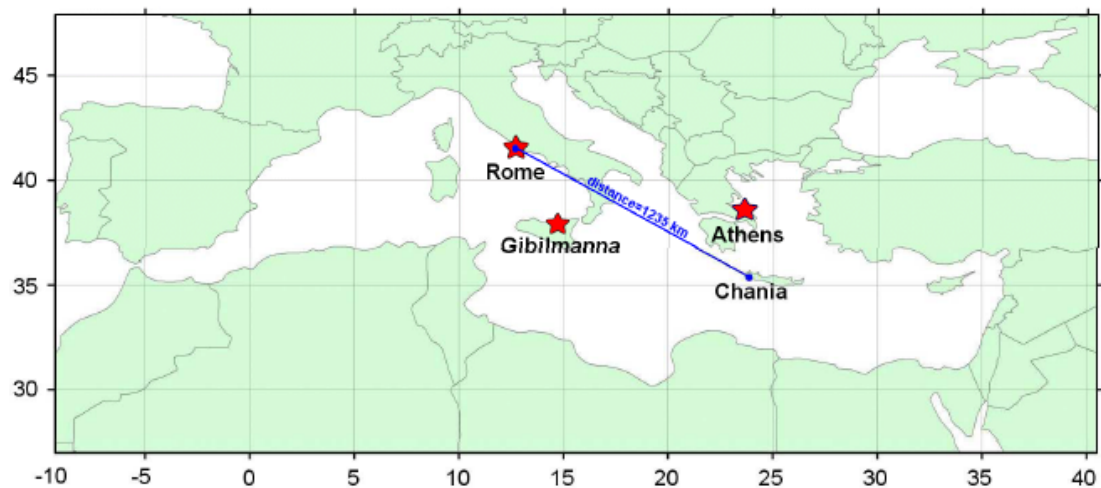


Figure 1. Map of the central Mediterranean region considered in this study. Red stars represent the ionospheric stations used as input for the ISP model. In blue, the radio link between Rome and Chania used to test the effectiveness of the IONORT-ISP system.

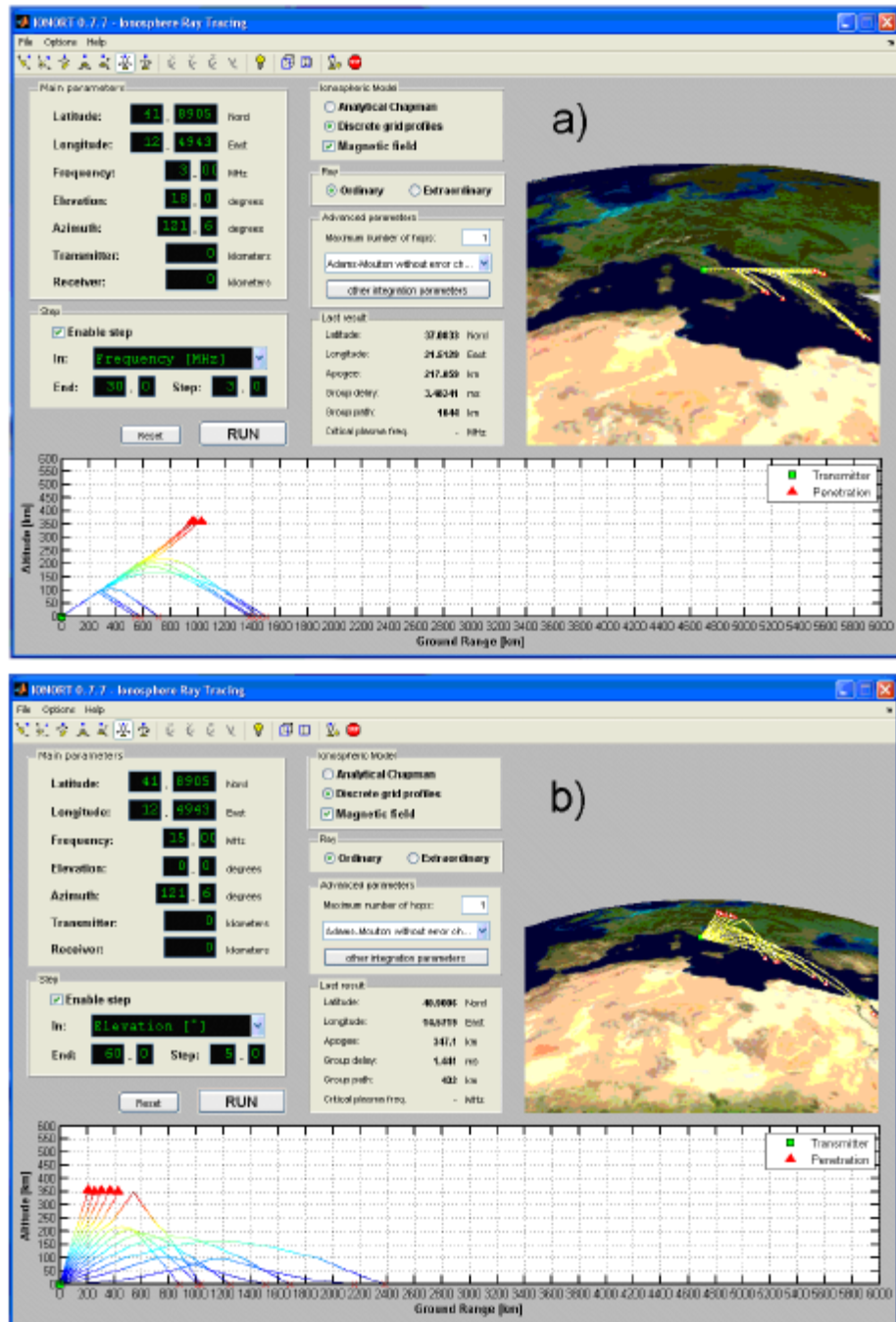


Figure 2. GUI of IONORT program. The 2-D and 3-D visualizations of the ray paths are shown at the bottom and right respectively, considering a transmitter point at Rome and an azimuth angle of transmission equal to 121.6° , in the direction of Chania. Two simulations are shown: a) for a fixed elevation angle equal to 18° with a 3 MHz frequency-step procedure from 3 MHz to 30 MHz; b) for a fixed frequency equal to 15 MHz with a 5° elevation-step procedure from 0° to 60° .

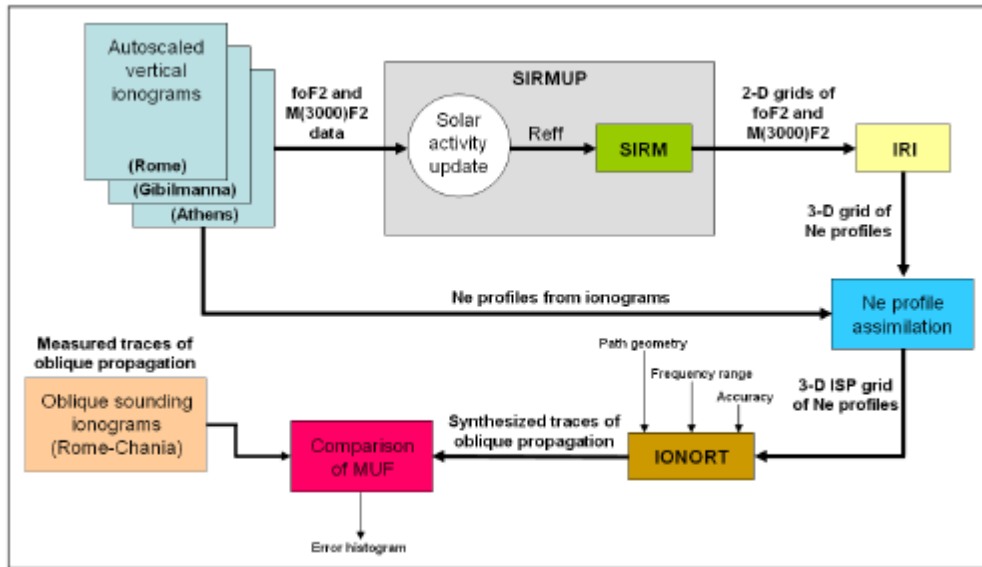


Figure 3. Overall chart of the IONORT-ISP system.

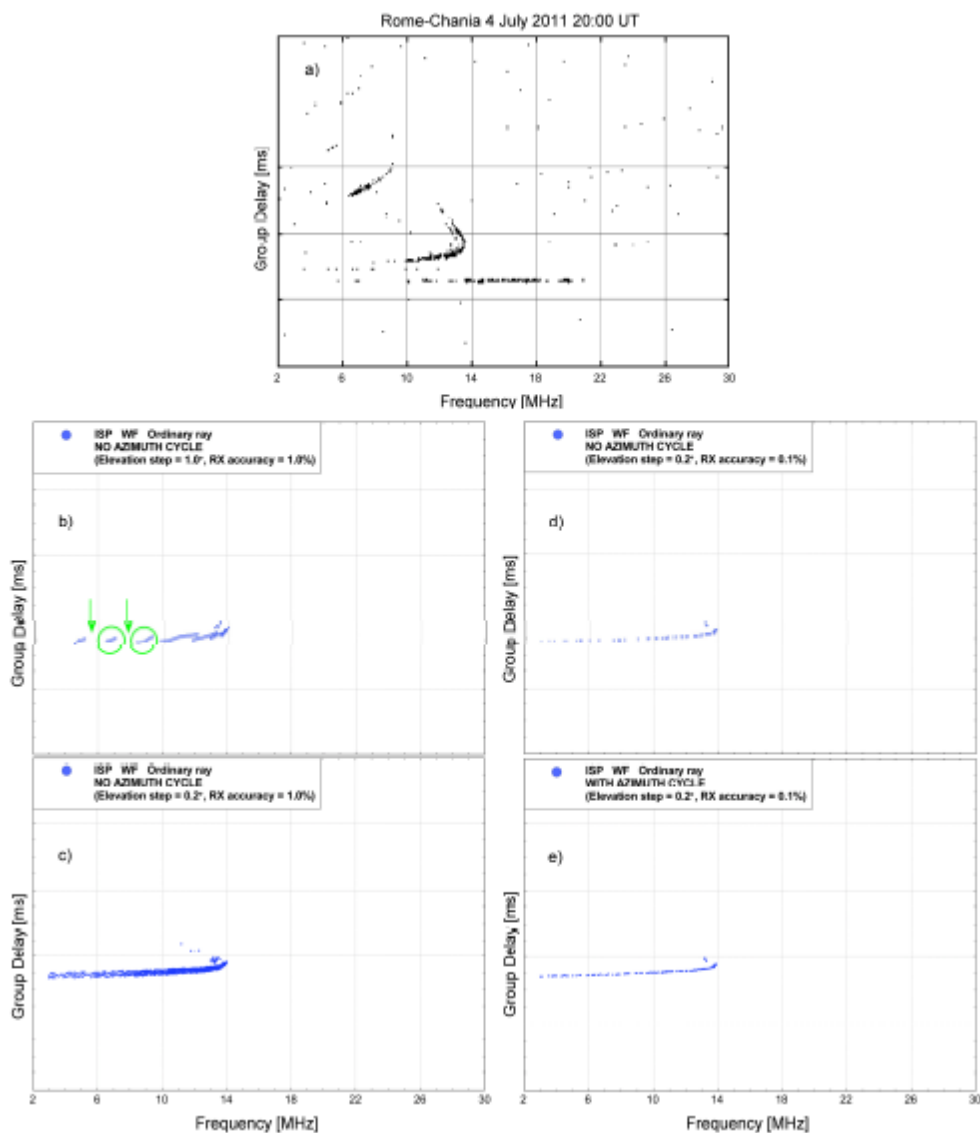


Figure 4. a) Oblique ionogram recorded over the Rome-Chania radio link on 4 July 2011 at 20:00 UT. Corresponding ordinary trace of the oblique ionograms synthesized by the IONORT-ISP system without applying the azimuth cycle with: b) the elevation angle step set to 1.0° and the RX range accuracy set to 1.0% (green circles and green arrows respectively highlight growing monotone trends and frequency gaps); c) the elevation angle step set to 0.2° and the RX accuracy set to 1.0%; d) the elevation angle step set to 0.2° and the RX accuracy set to 0.1%. e) Corresponding oblique ionogram synthesized by the IONORT-ISP system, after applying the azimuth cycle, with the elevation angle step set to 0.2° and the RX accuracy set to 0.1%. WF (with field) indicates that the synthesized ionograms were computed with taking the geomagnetic field into account.

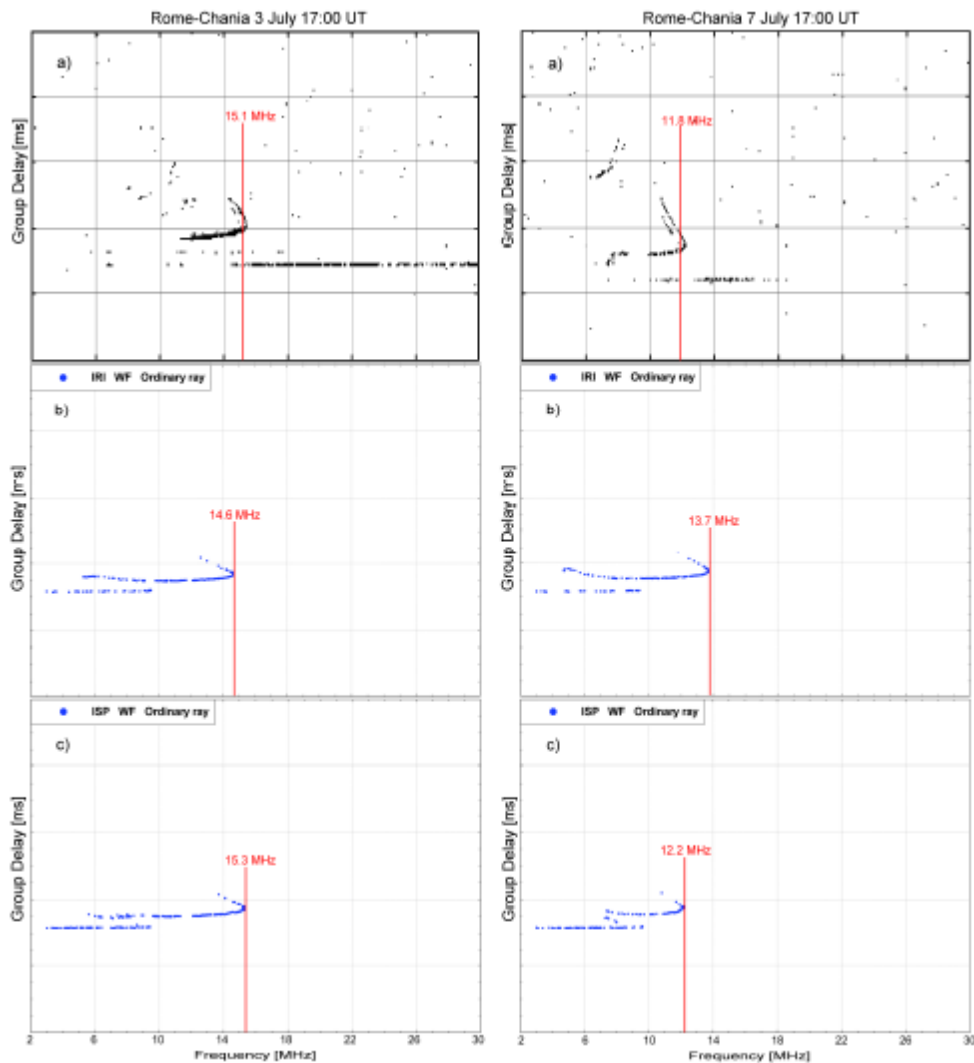


Figure 5. a) Oblique ionograms recorded over the Rome-Chania radio link on 3 July 2011 at 17:00 UT and 7 July 2011 at 17:00 UT. b) Ordinary trace of the ionograms synthesized by the IONORT-IRI system. c) Ordinary trace of the ionograms synthesized by the IONORT-ISP system after applying the azimuth cycle, and by setting the elevation angle step to 0.2° and the RX range accuracy to 0.1%. Vertical red lines identify the corresponding measured and synthesized MUF values. WF (with field) indicates that the synthesized ionograms were computed taking the geomagnetic field into account.

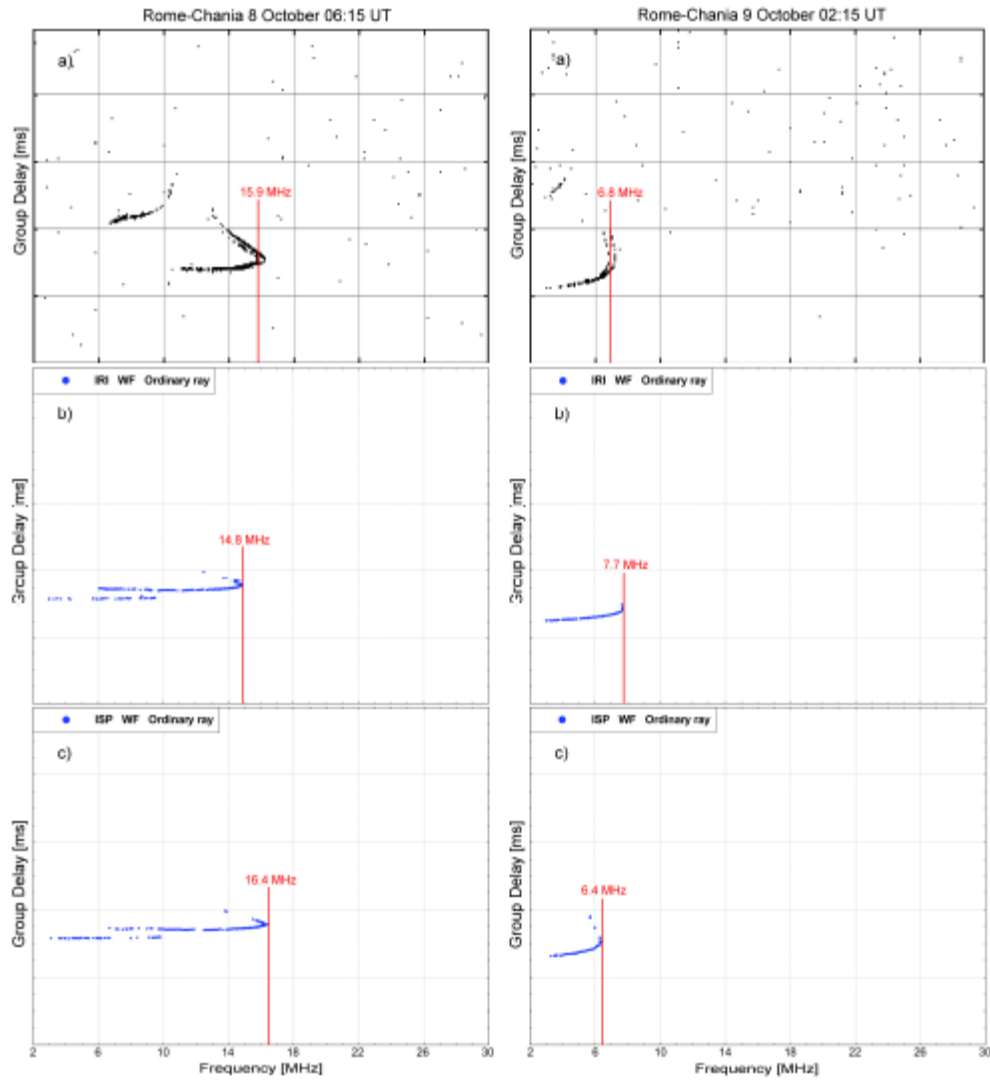


Figure 6. Same as Figure 5 for oblique ionograms recorded over the Rome-Chania radio link on 8 October 2011 at 06:15 UT and 9 October 2011 at 02:15 UT.

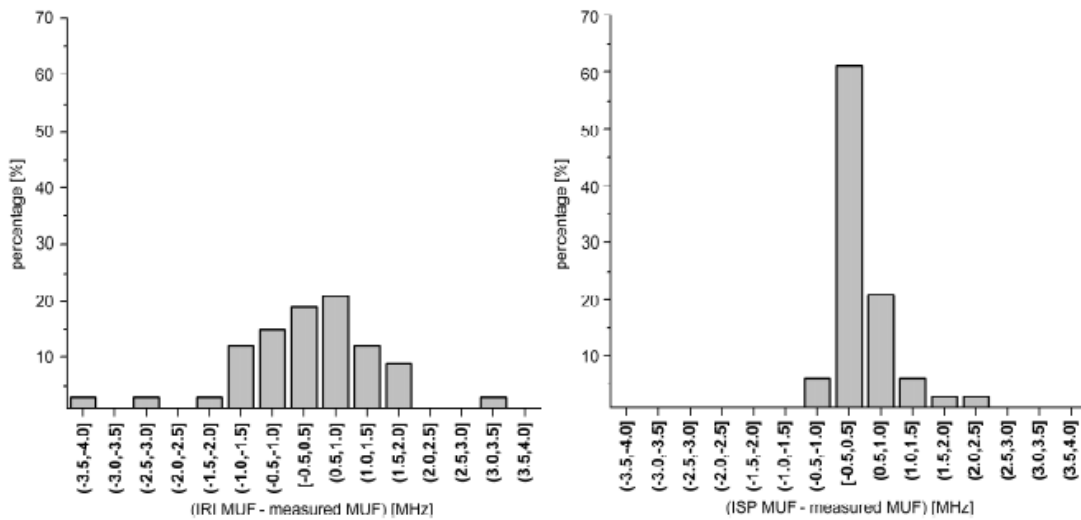


Figure 7. a) Differences between the MUF modelled by the IONORT-IRI system and the measured MUF. b) Differences between the MUF modelled by the IONORT-ISP system and the measured MUF.

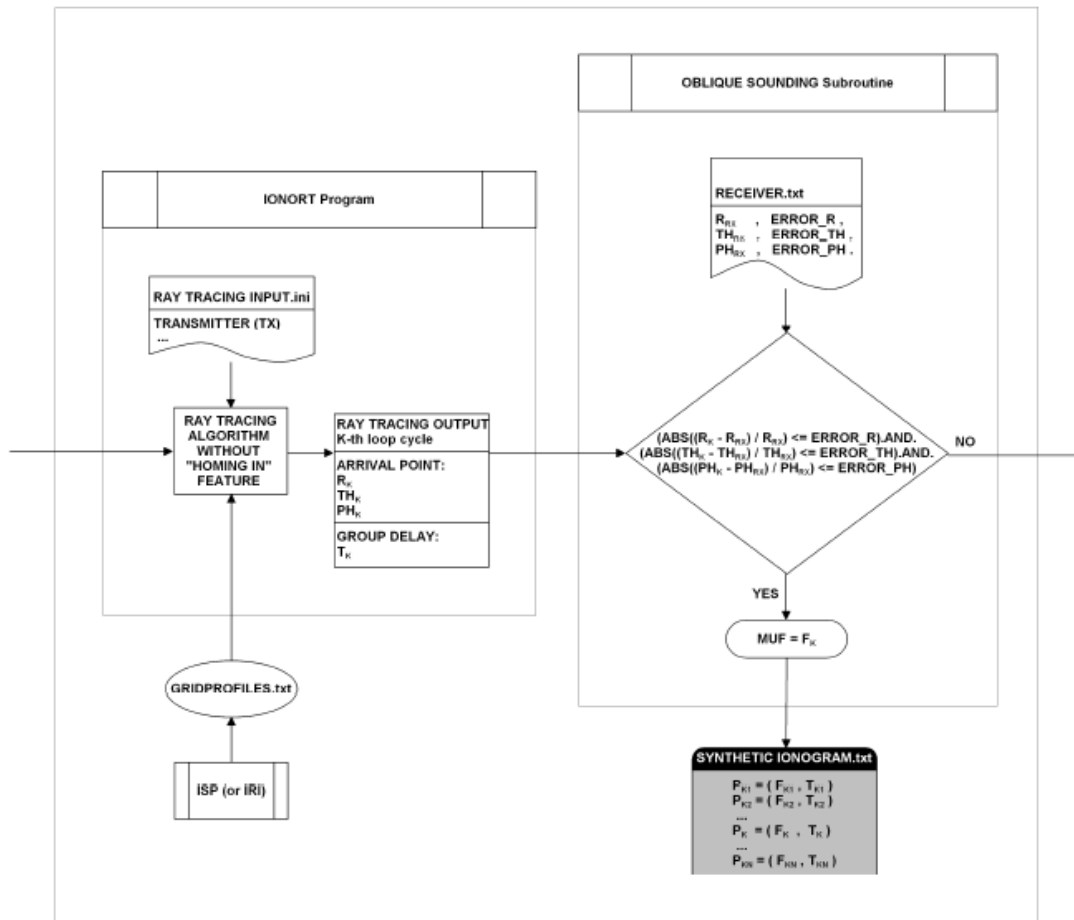


Figure A1b. Exploded details of the logical box shown at the centre of Figure A1a containing both the IONORT program and OBLIQUE SOUNDING subroutine.

Table 1. MUF calculated by the IONORT-IRI system (IRI MUF), MUF calculated by the IONORT-ISP system (ISP MUF), measured MUF, and the corresponding differences for all the ionograms of the test dataset. For each case, the lowest difference, between the modelled MUF (IONORT-IRI or IONORT-ISP) and the measured MUF, is highlighted in green.

Date and Time [UT]	IRI MUF [MHz]	ISP MUF [MHz]	MEASURED MUF [MHz]	(IRI MUF- MEASURED MUF) [MHz]	(ISP MUF- MEASURED MUF) [MHz]
23 JUN 2011 - 17:00	14.1	11.4	10.7	3.4	0.7
23 JUN 2011 - 19:00	13.1	15.1	14.9	1.8	0.2
23 JUN 2011 - 23:00	10.1	8.3	8.6	1.5	-0.3
25 JUN 2011 - 10:00	14.9	14.7	13.4	1.5	1.3
25 JUN 2011 - 20:00	12.4	13.1	13.4	-1.0	-0.3
25 JUN 2011 - 23:00	10.1	11.3	11.4	-1.3	-0.1
26 JUN 2011 - 00:00	9.7	8.8	9.0	0.7	-0.2
26 JUN 2011 - 01:00	9.2	8.9	8.8	0.4	0.1
26 JUN 2011 - 02:00	9.0	8.9	8.2	0.8	0.7
03 JUL 2011 - 17:00	14.6	15.3	15.1	-0.5	0.2
04 JUL 2011 - 19:00	13.2	13.9	13.8	-0.6	0.1
04 JUL 2011 - 20:00	12.3	13.9	13.2	-0.9	0.7
06 JUL 2011 - 12:00	14.9	14.5	13.7	1.2	0.8
06 JUL 2011 - 21:00	11.8	12.8	13.5	-1.7	-0.7
07 JUL 2011 - 01:00	9.2	8.0	8.3	0.9	-0.3
07 JUL 2011 - 14:00	13.9	13.8	12.4	1.5	1.4
07 JUL 2011 - 15:00	13.9	13.6	13.0	0.9	0.6
07 JUL 2011 - 17:00	13.7	12.2	11.8	1.9	0.4
07 JUL 2011 - 18:00	13.1	13.0	13.5	-0.4	-0.5
07 JUL 2011 - 19:00	13.1	13.6	14.0	-0.9	-0.4
08 JUL 2011 - 17:00	13.9	12.2	12.1	1.8	0.1
08 JUL 2011 - 18:00	13.0	14.6	14.5	-1.5	0.1

08 JUL 2011 - 19:00	13.1	15.8	16.7	-3.6	-0.9
08 OCT 2011 - 06:15	14.8	16.4	15.9	-1.1	0.5
08 OCT 2011 - 06:45	15.0	18.3	17.7	-2.7	0.6
08 OCT 2011 - 10:30	19.5	20.4	20.5	-1.0	-0.1
08 OCT 2011 - 20:00	9.4	9.0	9.2	0.2	-0.2
08 OCT 2011 - 23:45	7.7	6.9	7.7	0.0	-0.8
09 OCT 2011 - 02:00	7.8	6.5	6.9	0.9	-0.4
09 OCT 2011 - 02:15	7.7	6.4	6.8	0.9	0.4
09 OCT 2011 - 03:00	7.4	6.8	6.7	0.7	0.1
09 OCT 2011 - 05:00	10.9	14.1	12.2	-1.3	1.9
09 OCT 2011 - 06:30	15.1	17.5	15.1	0.0	2.4
